



Analysis of a K_a-Band Downlink System for Earth Observation Satellites

KEYWORDS

K_a-band propagation
Satellite downlink
Ground station visibility
Earth observation

ABSTRACT

Earth observation missions that are already slated for launch in the near future are expected to collect a massive daily data volume, requiring an adequate communication architecture to support their transmission to Earth at very high rates. In order to attain such requirements, K_a-band downlink is currently deemed as the most promising strategy. The effects of transmitting at a much higher frequency, compared to the vast majority of current satellites, must be taken into account, especially in terms of atmospheric attenuation. For the ground segment, already existing Earth sites are selected from NASA's Near Earth Network. Even though, almost of all them do not currently support K_a-downlink, an upgrade of these facilities is being considered by NASA. In this study, the choice of the proposed set of ground stations is supported by orbit simulations aimed at evaluating visibility and downlink budget. Based on a detailed analysis of the overall attenuation affecting the links, a preliminary design of the spaceborne antenna is also performed.

1 Introduction

The data volume acquired by current and future generation of Earth observation sensors is rapidly escalating. All of this is creating an increasing amount of data which has to be delivered from space to ground.

There are two approaches to support this need: increasing space-to-ground contact time, resulting in a more complex ground station network (GSN), or increasing carrier frequency which nevertheless impairs link reliability due to atmospheric effects.

For the sensor instrument of our reference mission we assumed a Synthetic Aperture Radar (SAR) operating in a Sun-synchronous Low Earth Orbit (LEO). Considering an average data volume of tens of Terabits per day, a K_a-band carrier frequency has been selected. In particular, the value $f = 26.25$ GHz has been chosen according to the available frequency allocations for European Earth exploration-satellites, established by the latest World Radiocommunication Conference [WRC19]. For the transmitted signal a dual channel circular-polarization has been selected.

A detailed model of the atmospheric propagation has been implemented in order to evaluate the minimum number of ground stations (G/Ss) required to fulfill the requirement of downlink budget.

The remainder of this paper is organized as follows: in Sec. 2 a comprehensive model of the signal attenuation due to the atmosphere is proposed. In Sec. 3 the reference orbit is

defined and aspects like the selection and the visibility of G/Ss are addressed. The discussion aims at proposing a solution to fulfill high throughput needs. The orbit of the spacecraft (S/C) is propagated accounting for the J_2 effect, which allows to accurately evaluate the transmission performance. In addition, an overall link budget analysis is presented, along with a preliminary sizing of the space segment. The final conclusions can be found in Sec. 4.

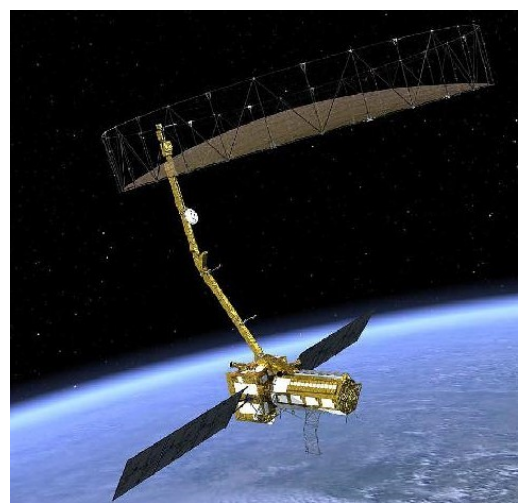


Figure 1: Artist's concept of the deployed NASA-ISRO NISAR spacecraft (image credit: NASA/JPL-Caltech)

2 Atmospheric Propagation

In the design of Earth-space links for communication systems, the effect of multiple sources of simultaneously occurring atmospheric attenuation must be considered. The overall attenuation represents the combined effect of:

- gaseous attenuation due to water vapour and oxygen
- attenuation due to rain
- attenuation due to clouds
- attenuation due to tropospheric scintillation

All these contributions depend on p , the probability that a given attenuation level is exceeded. The value $p = 1\%$ has been considered as an acceptable threshold for sizing our communication architecture.

Ionospheric effects may be important at frequencies below 1 GHz, while above 10 GHz (i.e. in our case) they are negligible.

Being the satellite a non-geostationary system, the effect of varying elevation angle to the S/C, θ , is relevant: the lower θ , the higher the attenuation. In particular, it is assumed that a minimum elevation of 5° is required for establishing a link with the G/S.

In other words, the most critical condition for designing the space segment will be the attenuation level in correspondence of $\theta = 5^\circ$, that is exceeded for 1% of an average year at each Earth station.

Prediction methods required for the design have been implemented according to [ITU17c]; for all the equations in the remainder of our discussion f has to be expressed in GHz.

2.1 Gaseous Attenuation

In order to estimate the attenuation of atmospheric gases along slant paths, an approximate method provided by [ITU19a] has been implemented, valid in the frequency range 1 – 350 GHz.

This method requires the following parameters, measured at the Earth surface, in correspondence of the G/S location:

- T : temperature
- p : pressure
- ρ : water vapour density

If local data is not available, a combination of the mean annual global reference atmosphere given in [ITU17d] can be used to estimate the T and p values (see Figs. 2 and 3), and maps of ρ at Earth surface vs. exceedance probability can be found in [ITU17e].

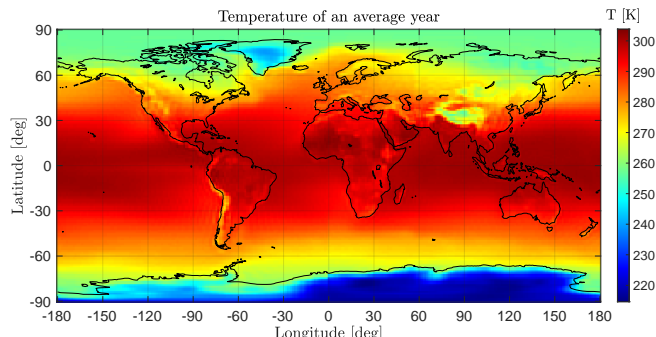


Figure 2: Mean annual temperature distribution at Earth surface

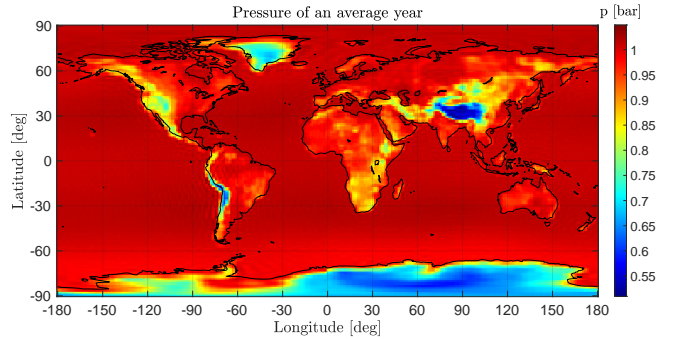


Figure 3: Mean annual pressure distribution at Earth surface

- i) The specific attenuation γ due to oxygen (o) and water vapour (w) can be accurately evaluated at any location using the individual spectral lines from each gas, considering small additional factors for the non-resonant Debye spectrum of oxygen below 10 GHz, pressure-induced nitrogen attenuation above 100 GHz and a wet continuum to account for the excess water vapour-absorption found experimentally. This model is applicable to frequencies up to 1000 GHz, and γ can be predicted as

$$\gamma_j = 0.1820 \cdot f \cdot N_j, \quad \text{where } j = o, w$$

where $N_o(f)$ and $N_w(f)$ are the imaginary parts of the frequency-dependent complex refractivities:

$$N_o(f) = \sum_i (\text{Oxygen}) S_i F_i + N_D \quad (1)$$

$$N_w(f) = \sum_i (\text{Water Vapour}) S_i F_i \quad (2)$$

S_i is the strength of the i -th oxygen or water vapour line, F_i is line shape factor (data from [ITU19a]).

$N_D(f)$ is the dry continuum due to pressure-induced nitrogen absorption and the Debye spectrum and as well as S_i is a function of f , T , dry air pressure and water vapour partial pressure.

Fig. 4 shows the specific attenuation, computed from 0 to 1000 GHz, for a mid-latitude location ($p = 1013.25 \text{ hPa}$, $T = 15^\circ \text{C}$).

Three cases are plotted: $\rho = 7.5 \text{ g/m}^3$ (Standard), dry atmosphere (Oxygen) and considering the water vapour contribution only (Water vapour).

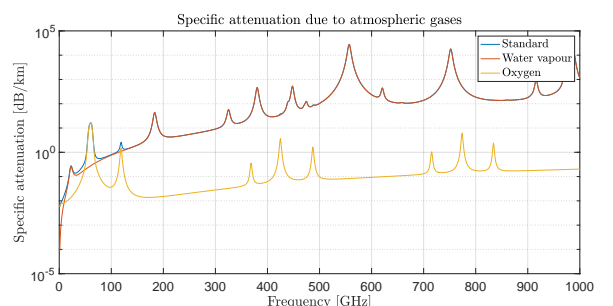


Figure 4: Gaseous specific attenuation

- ii) The estimation of the link loss caused by atmospheric gases along slant paths through the Earth's atmosphere is based on the concept of equivalent heights (h_o and h_w) by which the specific attenuation are multiplied to obtain the zenith attenuation. The equivalent heights depend on T , p and ρ , and are computed assuming an exponential atmosphere specified by a scale height to describe the decay in density with altitude [ITU19a].

- iii) For $5^\circ \leq \theta \leq 90^\circ$, the gaseous attenuation in Earth-space paths can be modeled as

$$A = \frac{A_o + A_w}{\sin \theta}$$

where the zenith attenuations for each gas are:

$$A_o = \gamma_o \cdot h_o, \quad A_w = \gamma_w \cdot h_w.$$

The resulting gaseous attenuation map at $\theta = 5^\circ$ is represented in Fig. 5.

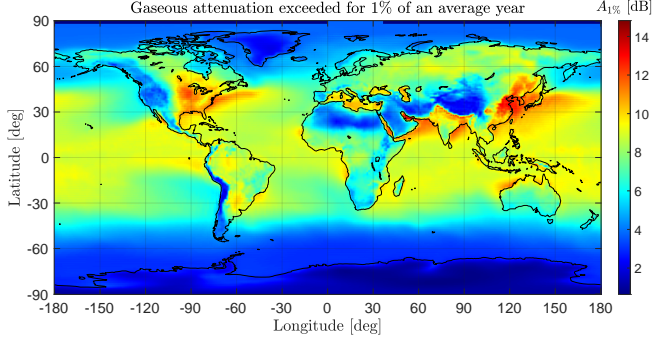


Figure 5: World map of the gaseous attenuation exceeded for 1% of an average year

2.2 Rain Attenuation

For the prediction of precipitation attenuation along a slant propagation path, a method valid for frequencies up to 55 GHz has been developed. A detailed description of the model can be found in [ITU17c]. The following parameters are required

$R_{0.01}$: rainfall rate exceeded for 0.01% of an average year

h_S : altitude of the G/S

ϕ : latitude of the G/S

θ : elevation angle of the S/C

- i) A digital map of the mean annual rain height h_R is provided in [ITU13] and represented in Fig. 6.

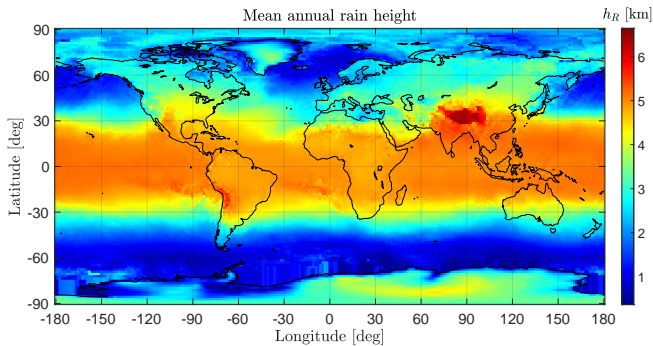


Figure 6: Mean annual rain height (ITU-R P.839)

- ii) The slant path length can be computed as

$$L_s = \begin{cases} \frac{h_R - h_S}{\sin \theta} & (\theta \geq 5^\circ) \\ \frac{2(h_R - h_S)}{\sqrt{\sin^2 \theta + \frac{2(h_R - h_S)}{R_{\text{eff}}}} + \sin \theta} & (\theta < 5^\circ) \end{cases}$$

where $R_{\text{eff}} = 8500$ km denotes Earth's effective radius.

Then the corresponding horizontal projection is given by $L_G = L_s \cos \theta$.

- iii) A digital map of the mean annual rainfall rate exceeded for 0.01% of an average year is provided in [ITU17a] and represented in Fig. 7.

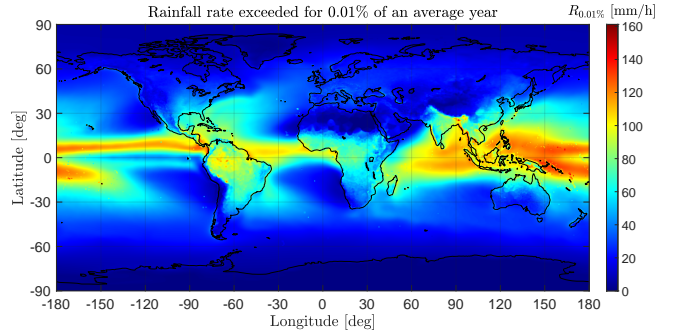


Figure 7: Mean annual rainfall rate (ITU-R P.837)

- iv) The specific attenuation γ_R [dB/km] can be determined using the power law

$$\gamma_R = k R_{0.01}^\alpha$$

where the computation of the fitting coefficients k and α is explained in [ITU05]. They will depend on frequency, elevation and polarization tilt angle (the latter corresponds to $\tau = 45^\circ$ for circular polarization).

- v) The predicted attenuation exceeded for 0.01% of an average year at a given location is obtained from

$$A_{0.01} = \gamma_R L_E$$

where L_E is called the effective path length and depends on the previously computed parameters.

- vi) One may at this point extrapolate the value of attenuation exceeded for an arbitrary percentage of the year, in the range 0.001% to 5%. In our case we will consider $p = 1$ (i.e. 1%) and compute:

$$A_p = A_{0.01} \left(\frac{p}{0.01} \right)^{[-0.655 + 0.033 \ln(p) - 0.045 \ln(A_{0.01} - \beta(1-p) \sin \theta)]}$$

where

$$\beta = \begin{cases} 0 & \text{if } p \geq 1\% \text{ or } |\phi| \geq 36^\circ \\ -0.005(|\phi| - 36^\circ) & \text{if } p < 1\%, |\phi| < 36^\circ, \theta \geq 25^\circ \\ -0.005(|\phi| - 36^\circ) + 1.8 - 4.25 \sin \theta & \text{otherwise} \end{cases}$$

As a final result, in correspondence of $\theta = 5^\circ$, the rain attenuation map in Fig. 8 is obtained.

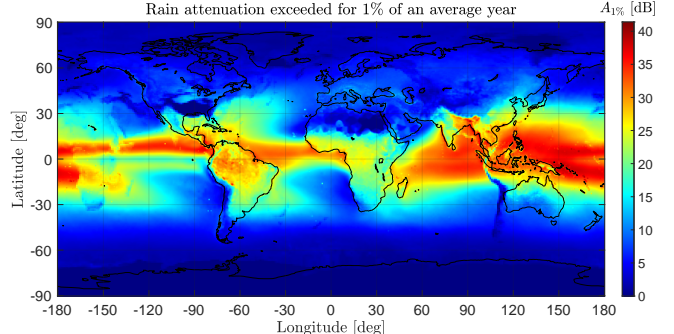


Figure 8: World map of the rain attenuation exceeded for 1% of an average year

2.3 Cloud Attenuation

The model here described can be found in [ITU19b] and is based on Rayleigh's approximation. The latter can be deemed valid for clouds/fog consisting of small droplets (i.e. diameter < 100 μm) and frequencies up to 200 GHz.

- i) A digital map of the cloud liquid water content L_{red} , reduced to a fixed temperature $T = 273.15$ K and exceeded for 1% of an average year, is provided in [ITU19b] and reported in Fig. 9.

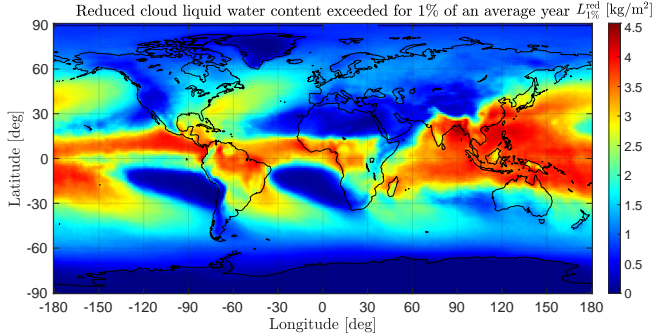


Figure 9: Reduced cloud liquid water content (ITU-R P.840)

- ii) The specific attenuation coefficient can be computed as

$$K_l(f, T) = \frac{0.819f}{\varepsilon'' \left[1 + \left(\frac{2 + \varepsilon'}{\varepsilon''} \right)^2 \right]}$$

where ε' and ε'' denote the real and imaginary part of water's complex dielectric permittivity, respectively.

- iii) Assuming an elevation angle greater or equal than 5° , the corresponding attenuation is determined from

$$A_{1\%} = \frac{L_{1\%} K_l}{\sin |\theta|}$$

The resulting cloud attenuation map at $\theta = 5^\circ$ is represented in Fig. 10.

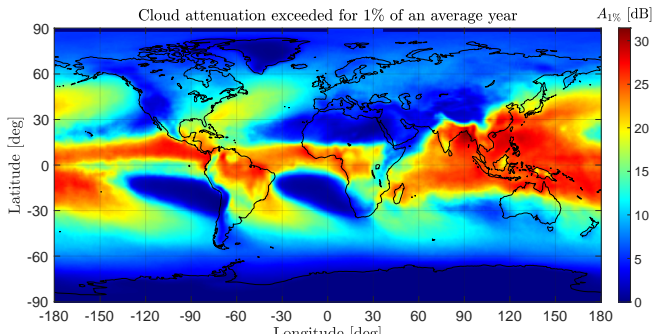


Figure 10: World map of the cloud attenuation exceeded for 1% of an average year

2.4 Scintillation Attenuation

The amplitude of tropospheric scintillations depends on the magnitude and structure of the refractive index variations along the propagation path. Amplitude scintillations increase with frequency and with the path length, and decrease as the antenna beamwidth decreases. Measured data shows that monthly-averaged root mean square fluctuations are well-correlated with the wet term of the radio refractivity N_{wet} , which depends on the water vapour content of the atmosphere.

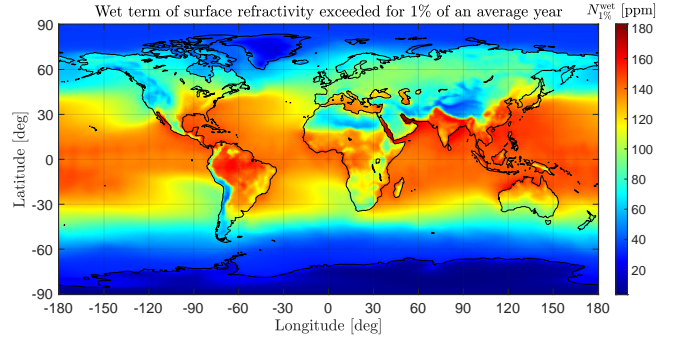


Figure 11: Mean annual distribution of N_{wet} (ITU-R P.453)

Another parameter required for the method is the apparent elevation angle that accounts for atmospheric refraction, always greater than the free-space elevation angle, which only considers the line-of-sight between the two stations [ITU17b]. The prediction method for the fading due to amplitude scintillation can be found in [ITU17c] and it is divided in three parts:

1. For free-space elevation angles $\theta \geq 5^\circ$ the scintillation fading $A(p)$, exceeded for $p\%$ of the time at the desired apparent elevation angle is the product between $a(p)$, the time percentage factor, and σ , the standard deviation of the signal for the applicable period and propagation path.
2. For fades $A \geq 25$ dB $A(p)$ is computed as a function of the apparent elevation angle and of the geoclimatic factor K_w for the average annual worst month [ITU19c].
3. In the transition region between the above two distributions, $A(p)$ is calculated by interpolating between the points $(\theta_1, A_1 = 25$ dB) and $(\theta_2 = 5^\circ, A_2)$ using a cubic exponential model.

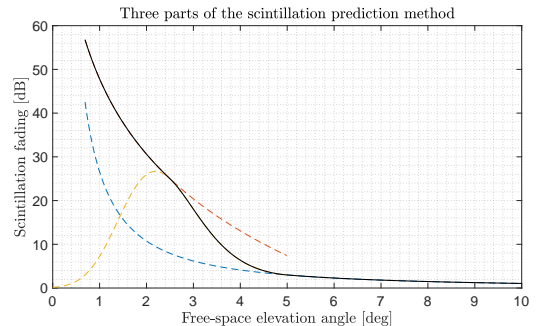


Figure 12: Scintillation attenuation models

In correspondence of $\theta = 5^\circ$, the resulting scintillation attenuation map is shown in Fig. 13.

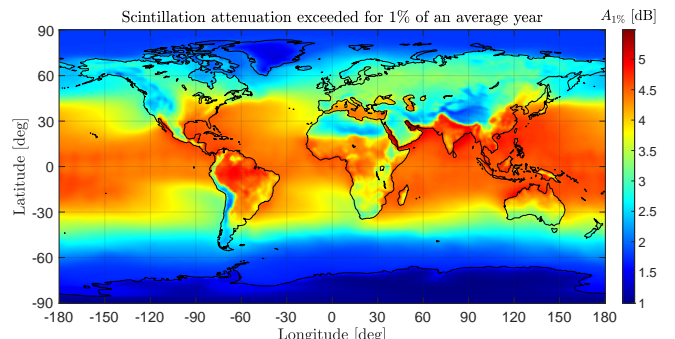


Figure 13: World map of the scintillation attenuation exceeded for 1% of an average year

2.5 Total Atmospheric Attenuation

The overall attenuation for a given probability level p can be evaluated using the following formula:

$$A_{\text{tot}}(p) = A_{\text{gas}}(p) + \sqrt{[A_{\text{rain}}(p) + A_{\text{cloud}}(p)]^2 + A_{\text{scint}}^2(p)}$$

The resulting map of the atmospheric attenuation being ex-

ceeded with a probability of 1% and given a 5° elevation, is provided in Fig. 14, along with the selected G/S sites. The choice of the latter will be later explained in more detail. It is evident that mid/high latitudes are highly favored, especially whenever a dry climate is usual. On the contrary, a G/S placed in an equatorial region would suffer a huge atmospheric attenuation that may translate in relatively frequent outages. This partly explains the choice of the Earth stations here highlighted.

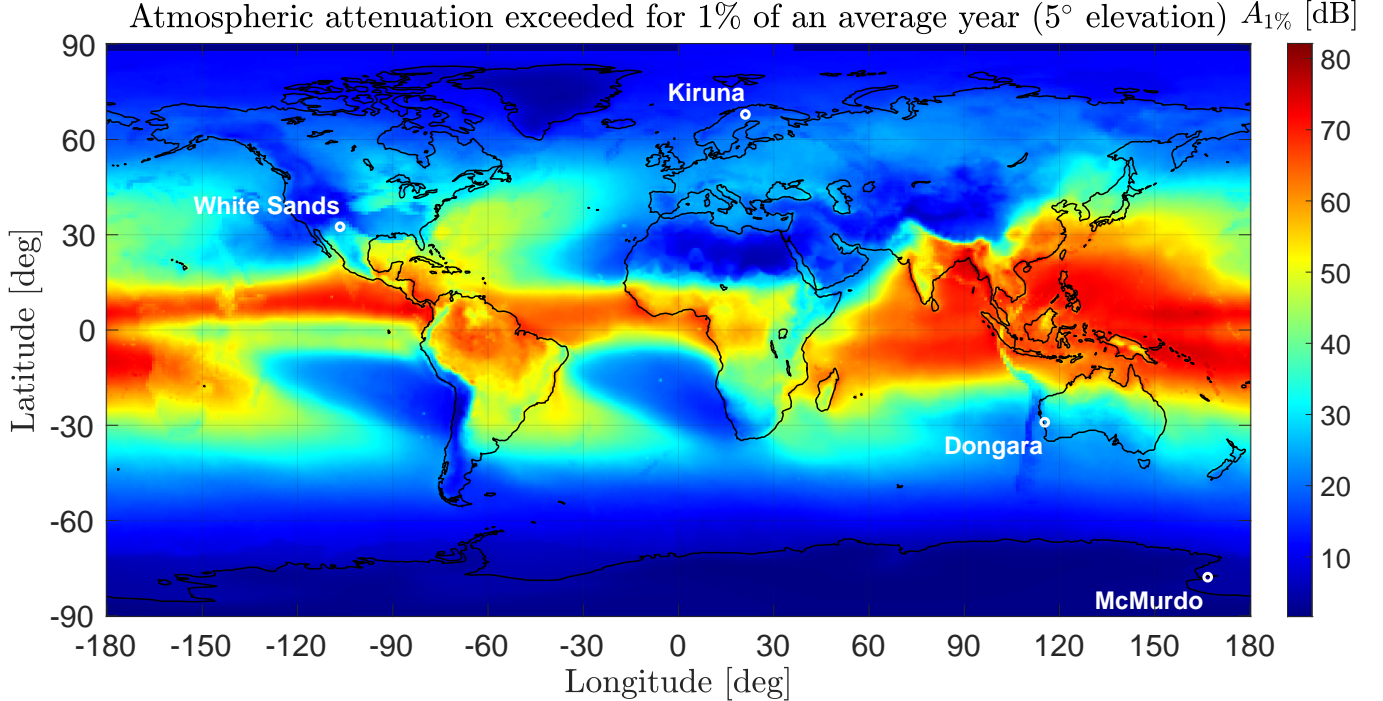


Figure 14: World map of the overall atmospheric attenuation exceeded for 1% of an average year

3 Downlink Budget

3.1 Orbit Definition

A basic requirement of Earth observation satellites is that of ensuring a fixed angle between the orbital plane and the Sun direction, which is achieved by means of a Sun-synchronous orbit. In addition, it is clear that the operation of the scientific payload will require a circular orbit (i.e. $e = 0$).

Once the semi-major axis a and the eccentricity e of the orbit are fixed, the corresponding inclination required to achieve a Sun-synchronous orbit is given by the following equation, whose derivation can be found in [Val01]:

$$\cos i = -a^{7/2} \cdot \frac{2 \left(\frac{360}{365.2421897} \cdot \frac{\frac{\pi}{180}}{86400} \right) (1 - e^2)^2}{3R_E^2 J_2 \sqrt{\mu}}$$

where J_2 denotes the first zonal harmonic (due to Earth's oblateness), while μ is the gravitational parameter of Earth.

After an iterative procedure aimed at designing an orbit that is also characterized by a repeating ground track, the following orbital elements have been selected:

$$a = 7186.6296 \text{ km} \quad e = 0 \quad i = 98.639^\circ$$

The resulting repeat-cycle has a duration of 4 days.

3.2 G/S Selection

As already stated in 2.5, in order to guarantee a low atmospheric attenuation during data download, equatorial G/Ss should be avoided.

In addition, given the near-polar orbit inclination, which is typical of all remote sensing missions, it turns out to be advantageous to pick G/S sites that are located either in the Arctic or Antarctic region. Indeed, the S/C will cross both the polar regions once per orbit, which increases the average contact time, besides the fact that very low attenuation levels are typical of high latitudes.

It was chosen to rely upon NASA's Near Earth Network (NEN) for the whole ground segment. A detailed datasheet of all available sites is provided in [Har14]. None of them is currently supporting K_a -band, except the White Sands station. Within the framework of performing the analysis of a future mission that might be slated for launch in the mid 2020s, it is nevertheless envisioned a scenario in which all available sites will be upgraded to support K_a downlink. For the purpose of our simulation, the same figure of merit G/T currently reported for X-band at each station will be assumed.

It was chosen to set a daily throughput of at least 40 Tbit/d as performance goal, which might be considered a reasonable estimate of the data rate that future SAR antennas might be able to acquire. For instance, NASA's NISAR mission will collect 35 Tbit per day of science data [Kob19]

and it is currently slated for launch during late 2022. As we will prove in the remainder of this section, the selection of the G/Ss in Tab. 1 allows to fulfill such a requirement.

Table 1: Main characteristics of the selected G/S sites

	Coordinates	Altitude [m]	Antenna Diameter [m]	G/T [dB/K]
Kiruna	67.8896 N 21.0657 E	402.2	13.0	33.0
McMurdo	77.8391 S 166.6671 E	206.4	10.0	32.0
Dongara	29.0457 S 115.3487 E	250.0	13.0	37.7
White Sands	32.5047 N 106.6108 W	1485.0	18.3	46.0

3.3 G/S Visibility & Daily Throughput

A simple model for determining the satellite-to-site elevation angle requires to compute two vectors $\underline{r}_{S/C}$ and $\underline{r}_{G/S}$ from the Earth's center to the S/C and to the G/S, respectively. Then, let $\Delta\underline{r} := \underline{r}_{S/C} - \underline{r}_{G/S}$ one may easily obtain that

$$\theta = \arcsin\left(\frac{\Delta\underline{r}}{\|\Delta\underline{r}\|} \cdot \frac{\underline{r}_{G/S}}{\|\underline{r}_{G/S}\|}\right)$$

and whenever $\theta < 0$ this means that there is no line-of-sight.

Exploiting the circularity of the orbit, we may simply write $\underline{r}_{S/C}$ as a function of the sub-satellite point:

$$\underline{r}_{S/C} = a \begin{Bmatrix} \cos \phi_{S/C} \cos \lambda_{S/C} \\ \cos \phi_{S/C} \sin \lambda_{S/C} \\ \sin \phi_{S/C} \end{Bmatrix}$$

and similarly:

$$\underline{r}_{G/S} = r_{G/S} \begin{Bmatrix} \cos \phi_{G/S} \cos \lambda_{G/S} \\ \cos \phi_{G/S} \sin \lambda_{G/S} \\ \sin \phi_{G/S} \end{Bmatrix}$$

where the value of $r_{G/S}$ has been computed by taking into account the actual geoid shape of the Earth. In particular, this was done by considering the ideal ellipsoid defined by the WGS84 model, superimposed with the EGM96 model (which defines the deviation of the geoid shape from the ellipsoid).

Considering a minimum elevation of 5° , the resulting coverage mask is depicted in Fig. 16, along with the ground track corresponding to a full repeat-cycle. The orbit propagator developed for this purpose accounts for the presence of the perturbing acceleration due to the J_2 -effect, although it neglects the presence of air-drag, solar radiation pressure and Moon's attraction.

The attenuation plot in Fig. 17 is obtained by combining the above mentioned elevation map (provided as a function of the sub-satellite point) with the propagation models described in Sec. 2. In particular, the atmospheric attenuation as a function of the elevation at each site can be visualized in Fig. 15.

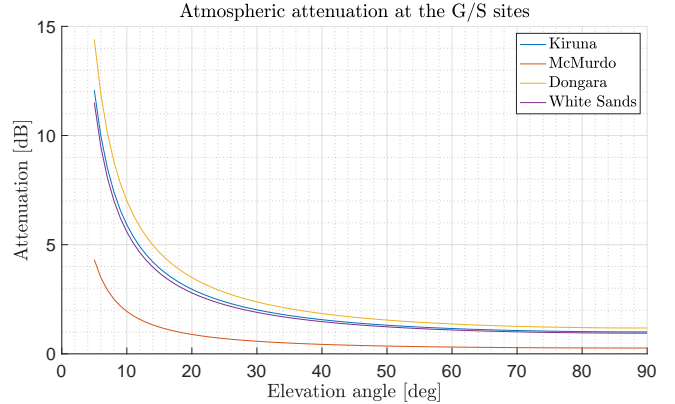


Figure 15: G/S attenuation map

In order to evaluate the daily data volume that can be downlinked to Earth, the orbit has to be propagated for a full repeat-cycle, due to the fact that the daily contact time will slightly differ depending on the cycle's progress. The history of sub-satellite points is then compared against the coverage map in Fig. 16, which easily allows to compute the contact time.

All passes shorter than 3 minutes are ruled out, i.e. they are not considered valid for establishing a stable space-to-Earth link.

At this point it is necessary to assume a transmission data rate for computing the overall throughput. The current state of the art is NASA/JPL's Universal Space Transponder - K_a -band Modulator (UST- K_a M), which is capable of transmitting up to 1.74 Gbit/s using OQPSK⁽¹⁾ modulation, with 7/8 LDPC⁽²⁾ correction coding [Pug18]. Operating two circular-polarized K_a channels will double the downlink rate, thus yielding a total of 3.48 Gbit/s.

The results of our simulation are summarized in Tab. 2. In particular it can be seen that the performance goal of 40 Tbit/d is largely met, achieving an average daily throughput of 74.86 Tbit.

It may appear that the two polar sites alone would suffice to achieve the required downlink volume, however, in practical operation the Solid State Recorder (SSR) fill/drain cycle introduces further constraints. Indeed the presence of two other mid-latitude G/S is fundamental to prevent data overflow in the SSR.

Table 2: Contact times & daily throughput

	Avg. Downlink Budget [Tbit/d]	Cycle Visibility	Avg. Daily Visibility
Kiruna	24.20	7 h 44 m (8.0%)	1 h 56 m
McMurdo	31.89	10 h 11 m (10.6%)	2 h 33 m
Dongara	9.26	2 h 58 m (3.1%)	0 h 44 m
White Sands	9.51	3 h 2 m (3.2%)	0 h 46 m
Total	74.86	23 h 55 m (24.9%)	5 h 59 m

⁽¹⁾Offset Quadrature Phase-Shift Keying

⁽²⁾Low-Density Parity Check

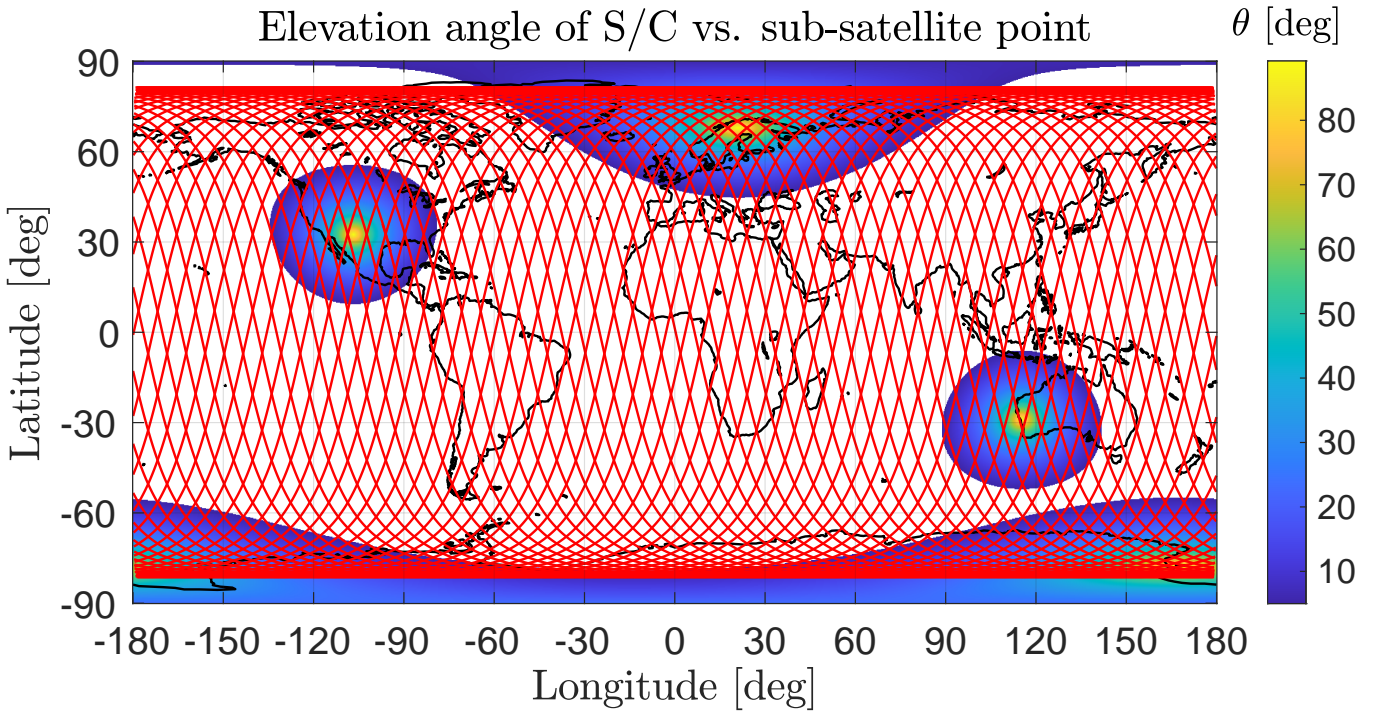


Figure 16: *G/S coverage map*

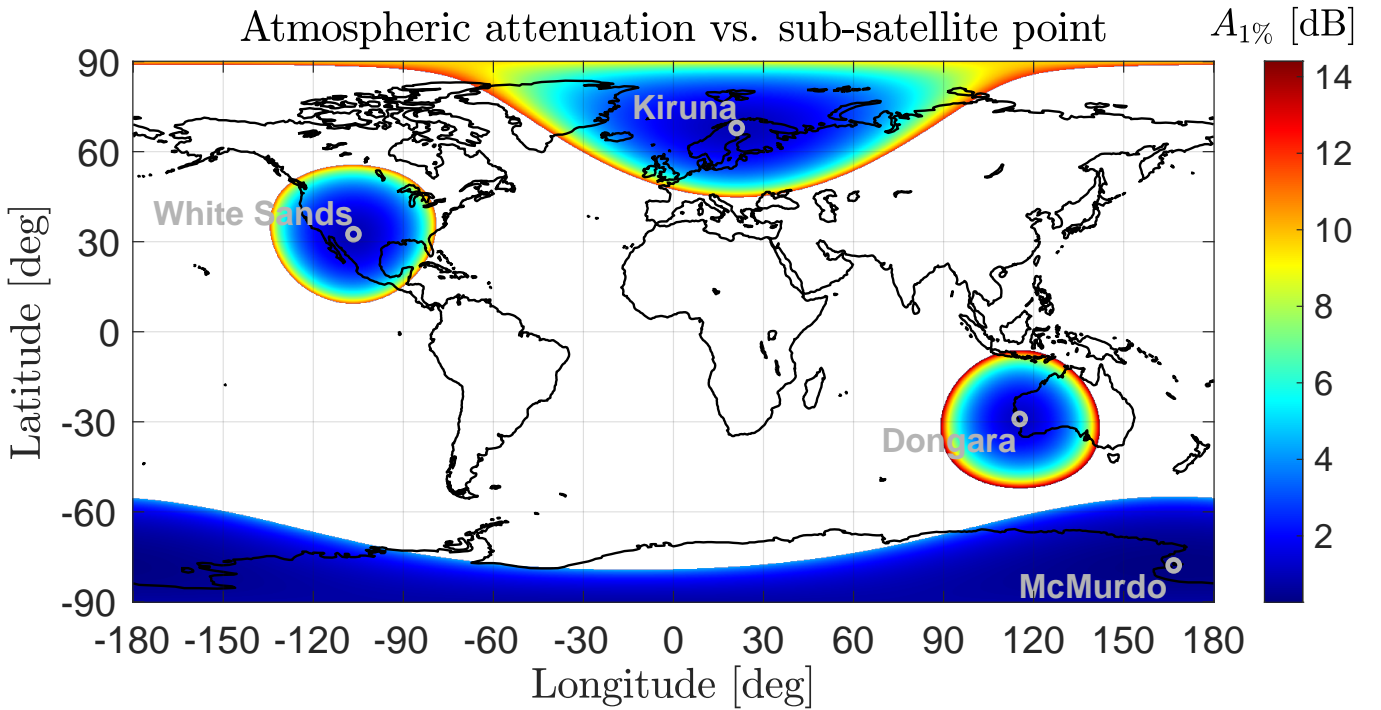


Figure 17: *G/S attenuation map*

3.4 Link Budget & Space Segment

The quality of a digital communication link can be measured in terms of Bit Error Rate (BER). The latter is directly related to the energy-per-bit to noise-power-density ratio, E_b/N_0 , by a relationship that depends on the specific coding and modulation techniques. In particular, as reported in [Div05], for a rate-7/8 LDPC coding scheme (i.e. the same used in UST-K_aM), the required E_b/N_0 for achieving $\text{BER} = 10^{-8}$ is about 4.1 dB. This will be set as the thresh-

old for sizing the TX-antenna. We will consider as usual the most critical operating conditions, at $\theta = \theta_{\min} \equiv 5^\circ$ and 1% weather. This also means that it should be accounted for the largest satellite-to-site distance for computing the free-space loss L_{FP} , namely

$$d_{\max} = -R_E \sin \theta_{\min} + \sqrt{(R_E \sin \theta_{\min})^2 + (a - R_E)^2 + 2R_E(a - R_E)} \\ = 2802.089 \text{ km}$$

$$L_{\text{FP}} = \frac{1}{\left(\frac{4\pi d_{\max}}{\lambda}\right)^2}$$

where $\lambda = 1.14$ cm denotes the wavelength of the carrier.

The atmospheric loss A_{atm} at each station is given by the initial value of the curves in Fig. 15.

The pointing loss in dB can be computed using the following formula, which is valid for a reflector antenna:

$$L^p = 12 \left(\frac{D_{\text{ant}} P^{\text{acc}}}{70\lambda} \right)$$

where P^{acc} is the pointing accuracy in degrees, and for TX it is assumed to be equal to 0.1° , which is a reasonable value according to [Sta11].⁽³⁾ The pointing accuracy of the ground antenna (RX) is instead already embedded in the figure of merit G_{RX}/T_n (or simply G/T), that is provided in the datasheets in [Har14].

The additional losses (e.g. circuit loss) L^{other} are assumed equal to -2.5 dB, both at TX/RX.

The gain in dB of the transmitting antenna can be calculated using the following formula, which holds true for a circular parabolic reflector:

$$G_{\text{TX}} = 10 \log_{10}(109.66 f^2 D_{\text{TX}}^2 \eta_{\text{TX}})$$

where f is expressed in GHz while a conservative estimate of the antenna efficiency might be $\eta_{\text{TX}} = 0.5$.

At this point, once the transmitted power and D_{TX} are fixed, the corresponding E_b/N_0 is easily obtained as

$$\begin{aligned} \frac{E_b}{N_0} &= \frac{B_n}{R_D} \cdot \text{SNR} \\ &= \frac{B_n}{R_D} \cdot \frac{P_{\text{TX}} G_{\text{TX}} L_{\text{TX}}^p L_{\text{TX}}^{\text{other}} \cdot G_{\text{RX}}/T_n L_{\text{RX}}^p L_{\text{RX}}^{\text{other}} \cdot A_{\text{atm}} L_{\text{FP}}}{K_b B_n} \end{aligned}$$

where

SNR: Signal-to-Noise Ratio (i.e. P_{RX}/P_n)

B_n : noise bandwidth

K_b : Boltzmann constant

R_D : data rate (3.48 Gbit/s)

Table 3: Link budget analysis ($D_{\text{TX}} = 1.0$ m, $P_{\text{TX}} = 5$ W)

[dB]	Kiruna	McMurdo	Dongara	White Sands
P_{TX}	6.99	6.99	6.99	6.99
G_{TX}	45.77	45.77	45.77	45.77
L_{TX}^p	-0.1875	-0.1875	-0.1875	-0.1875
$L_{\text{TX}}^{\text{other}}$	-2.50	-2.50	-2.50	-2.50
G_{RX}/T_n	33.00	32.00	37.70	46.00
L_{RX}^p	↑	↑	↑	↑
$L_{\text{RX}}^{\text{other}}$	-2.50	-2.50	-2.50	-2.50
A_{atm}	-12.08	-4.31	-14.41	-11.51
L_{FP}	-189.77	-189.77	-189.77	-189.77
$1/(K_b \cdot R_D)$	133.19	133.19	133.19	133.19
$\frac{E_b}{N_0}$	11.78	18.68	14.15	25.04
Required E_b/N_0	4.1	4.1	4.1	4.1
Link margin	7.68	14.58	10.05	20.94

⁽³⁾provided that sufficiently precise sensors (e.g. star trackers) and attitude control systems (e.g. reaction wheels or CMGs) are available onboard the S/C

The results in Tab. 3 are obtained by considering for the space segment a 1.0 m parabolic antenna with a transmit power per channel equal to $P_{\text{TX}} = 5$ W.

As it can be seen, the most critical G/S is the one located in Kiruna: this is basically due to a comparatively low figure of merit, along with a relatively high atmospheric attenuation. A link margin greater than 7.68 dB is hence guaranteed for all Earth stations.

4 Conclusions

The results presented in this paper demonstrate the feasibility of a LEO K_a -downlink capable of a daily throughput in the order of tens of Terabits. Considering current state of the art transmission hardware, a downlink budget of 74.86 Tbit/d was proved to be feasible by relying on a set of only four G/Ss.

Indeed, the upgrade of current facilities to support K_a -band turns out to be essential for fulfilling the requirements of SAR missions planned in the foreseeable future, without an extraordinary increase in the size of the GSN. The upgrade of Kiruna and McMurdo NEN sites should be considered as a priority, given that frequent polar region crossing is a common feature of all Earth observation missions.

Using a parabolic antenna with diameter of 1.0 m and RF power of 5 W per polarization, a link margin of 7.68 dB is guaranteed for all ground stations.

References

- [Ali99] Irfan Ali, Naofal Al-Dahir, and John E Hershey. “Predicting the visibility of LEO satellites”. In: *IEEE Transactions on Aerospace and Electronic Systems* 35.4 (1999), pp. 1183–1190.
- [Chr12] Jorn Christensen. “Itu regulations for ka-band satellite networks”. In: *30th AIAA International Communications Satellite System Conference (IC-SSC)*. 2012, p. 15179.
- [Dah17] Trevor A Dahl and Brian C Gunter. “An Evaluation of Spacecraft Pointing Requirements for Optically Linked Satellite Systems”. In: (2017).
- [Div05] Dariush Divsalar, Sam Dolinar, and Christopher Jones. “Low-rate LDPC codes with simple protograph structure”. In: *Proceedings. International Symposium on Information Theory, 2005. ISIT 2005*. IEEE. 2005, pp. 1622–1626.
- [Han17] Chao Han, XiaoJie Gao, and XiuCong Sun. “Rapid satellite-to-site visibility determination based on self-adaptive interpolation technique”. In: *Science China Technological Sciences* 60.2 (2017), pp. 264–270.
- [Har14] MA Harris. “Near Earth Network (NEN) Users’ Guide”. In: *Tech. Rep. 453-NENUG, NASA Exploration and Space Communications Projects Division* (2014).
- [Hen16] Hennes Henniger, Erhard Diedrich, and Stefan Seyfarth. “Analysis and comparison of new downlink technologies for earth observation satellites”. In: *Radioengineering* 25.1 (2016), pp. 1–11.
- [Ipp17] Louis J Ippolito. *Satellite communications systems engineering*. Wiley Online Library, 2017.

- [ITU05] Recommendation (ITU). “Specific attenuation model for rain for use in prediction methods”. In: *ITU-R P.838-3* (2005).
- [ITU13] Recommendation (ITU). “Rain height model for prediction methods”. In: *ITU-R P.839-4* (2013).
- [ITU17a] Recommendation (ITU). “Characteristics of precipitation for propagation modelling”. In: *ITU-R P.837-7* (2017).
- [ITU17b] Recommendation (ITU). “Effects of tropospheric refraction on radiowave propagation”. In: *ITU-R P.834-9* (2017).
- [ITU17c] Recommendation (ITU). “Propagation data and prediction methods required for the design of Earth-space telecommunication systems”. In: *ITU-R P.618-13* (2017).
- [ITU17d] Recommendation (ITU). “Reference standard atmospheres”. In: *ITU-R P.835-6* (2017).
- [ITU17e] Recommendation (ITU). “Water vapour: surface density and total columnar content”. In: *ITU-R P.836-6* (2017).
- [ITU19a] Recommendation (ITU). “Attenuation by atmospheric gases”. In: *ITU-R P.676-12* (2019).
- [ITU19b] Recommendation (ITU). “Attenuation due to clouds and fog”. In: *ITU-R P.840-8* (2019).
- [ITU19c] Recommendation (ITU). “The radio refractive index: its formula and refractivity data”. In: *ITU-R P.453-14* (2019).
- [Kob19] M Michael Kobayashi et al. “NASA’s high-rate Ka-band downlink system for the NISAR mission”. In: *Acta Astronautica* 159 (2019), pp. 358–361.
- [Kun14] Anindya Kumar Kundu et al. “Designing a mobile satellite communication Antenna and Link Budget Optimization”. In: *2013 International Conference on Electrical Information and Communication Technology (EICT)*. IEEE. 2014, pp. 1–6.
- [Lee05] Dennis Lee et al. “A gigabit-per-second Ka-band demonstration using a reconfigurable FPGA modulator”. In: *2005 IEEE Aerospace Conference*. IEEE. 2005, pp. 1370–1378.
- [Lew13] UJ Lewark et al. “Link budget analysis for future E-band gigabit satellite communication links (71–76 and 81–84 GHz)”. In: *CEAS Space Journal* 4.1-4 (2013), pp. 41–46.
- [McC10] Kevin McCarthy et al. “NASA’s evolution to ka-band space communications for near-earth spacecraft”. In: *SpaceOps 2010 Conference Delivering on the Dream Hosted by NASA Marshall Space Flight Center and Organized by AIAA*. 2010, p. 2176.
- [Pug18] Michael Pugh et al. “High-rate Ka-band modulator for the NISAR mission”. In: *2018 IEEE Aerospace Conference*. IEEE. 2018, pp. 1–13.
- [Sta11] Scott R Starin and John Eterno. “Attitude determination and control systems”. In: (2011).
- [Val01] David A Vallado. *Fundamentals of astrodynamics and applications*. Vol. 12. Springer Science & Business Media, 2001.
- [WRC19] World Radiocommunication Conference 2019 (WRC-19). “Provisional Final Acts”. In: (2019).
- [Xay15] Peter Xaypraseuth, R Satish, and Alok Chatterjee. “NISAR spacecraft concept overview: Design challenges for a proposed flagship dual-frequency SAR mission”. In: *2015 IEEE Aerospace Conference*. IEEE. 2015, pp. 1–11.
- [Zyr98] Jim Zyren and Al Petrick. “Tutorial on basic link budget analysis”. In: *Application Note AN9804, Harris Semiconductor* 31 (1998).